# Loss of β Epithelial Sodium Channel Function in Meibomian Glands Produces Pseudohypoaldosteronism 1—Like Ocular Disease in Mice

Dongfang Yu,*† Yogesh Saini,‡ Gang Chen,* Andrew J. Ghio,§ Hong Dang,* Kimberlie A. Burns,* Yang Wang,* Richard M. Davis,¶ Scott H. Randell,* Charles R. Esther, Jr,‖ Friedrich Paulsen,** and Richard C. Boucher*

*From the Marsico Lung Institute/University of North Carolina Cystic Fibrosis Research Center,* School of Medicine, and the Departments of Ophthalmology¶ and Pediatrics,‖ University of North Carolina at Chapel Hill, Chapel Hill, North Carolina; the Department of Pathology,† Wake Forest School of Medicine, Winston-Salem, North Carolina; the Department of Comparative Biomedical Sciences,‡ School of Veterinary Medicine, Louisiana State University, Baton Rouge, Louisiana; the National Health and Environmental Effects Research Laboratory,§ Environmental Protection Agency, Chapel Hill, North Carolina; and the Department of Anatomy II,** Friedrich Alexander University Erlangen Nürnberg, Erlangen, Germany*

Accepted for publication September 21, 2017.

Address correspondence to Richard C. Boucher, M.D., Marsico Lung Institute/University of North Carolina Cystic Fibrosis Research Center, School of Medicine, University of North Carolina at Chapel Hill, 130 Mason Farm Rd., 7008 Marsico Hall, Chapel Hill, NC 27599. E-mail: richard_boucher@med.unc.edu.

Human subjects with pseudohypoaldosteronism-1 because of loss-of-function mutations in epithelial sodium channel (ENaC) subunits exhibit meibomian gland (MG) dysfunction. A conditional *βENaC* MG knockout (KO) mouse model was generated to elucidate the pathogenesis of absent ENaC function in the MG and associated ocular surface disease. *βENaC* MG KO mice exhibited a striking age-dependent, female-predominant MG dysfunction phenotype, with white toothpaste—like secretions observed obstructing MG orifices at 7 weeks of age. There were compensatory increases in tear production but higher tear sodium and indexes of mucin concentration in *βENaC* MG KO mice. Histologically, MG acinar atrophy was observed with ductal enlargement and ductal epithelial hyperstratification. Inflammatory cell infiltration was observed in both MG and conjunctiva of *βENaC* MG KO mice. In older *βENaC* MG KO mice (5 to 11 months), significant ocular surface pathologies were noted, including corneal opacification, ulceration, neovascularization, and ectasia. Inflammation in MG and conjunctiva was confirmed by increased cytokine gene and protein expression and positive Ly-6B.2 immunostaining. Cell proliferation assays revealed lower proliferation rates of MG cells derived from *βENaC* MG KO than control mice, suggesting that βENaC plays a role in cell renewal of mouse MG. Loss of βENaC function resulted in MG disease and severe ocular surface damage that phenocopied aspects of human pseudohypoaldosteronism-1 MG disease and was sex dependent. *(Am J Pathol 2018, 188: 95—110; https://doi.org/10.1016/j.ajpath.2017.09.016)*

Meibomian glands (MGs) play a critical role in maintaining the health and homeostasis of the ocular surface. As modified sebaceous glands that reside within the upper and lower eyelids, MG acini secrete a lipid-rich mixture (meibum) via a holocrine mechanism into a pseudostratified duct.[1] The meibum is released onto the tear film, where it stabilizes the tear film and prevents evaporation. Compromise of meibum production and secretion, as occurs in meibomian gland dysfunction (MGD), results in a homeostatic imbalance of the tear film that damages the ocular surface.[2] This damage can include the physically contiguous, but morphologically distinct, epithelia covering the cornea, limbus, and conjunctiva.

MGD is a chronic, diffuse abnormality of the MG, commonly characterized by terminal duct obstruction and/or qualitative/quantitative changes in the glandular secretions.[3] It is well established that MGD is a leading cause of dry eye disease (DED), which afflicts 4 to 6 million individuals in the United States.[4,5] Several ophthalmic-, systemic-, and

Supported by NIH/National Heart, Lung, and Blood Institute grants BOUCHER P01HL110873, P01HL108808, R01HL136961, R01HL116228, and K23HL089708; and German Research Foundation DFG grant PA738/9-2.

Disclosures: S.H.R. received financial support from Parion Sciences and is a consultant at Gilead Sciences. R.C.B. is an investor in Parion Sciences.

medication-related factors have been reported to be correlated with MGD. Specific factors include age, sex, contact lens wear, anterior blepharitis, androgen deficiency, hormonal replacement therapy, and antihistamines.[2,6,7] Despite these observations, many questions remain about the pathogenesis and management of MGD.

Previous clinical observations in subjects with a genetic loss of epithelial sodium channel (ENaC) function [pseudohypoaldosteronism (PHA 1)] revealed prominent white collections at the orifices of MG, a pathognomonic abnormality of MGD.[8−10] ENaC, a multimeric sodium absorptive channel composed of α, β, and γ subunits, plays a pivotal role in ion transport physiology in the ductal epithelia of sweat and salivary glands.[11] The PHA 1 clinical observations, together with our recent findings of the expression of a broad profile of ion channels/transporters, including ENaC, in rat MG acini rather than ducts, suggested an unexplained role for ENaC in MG function.[12] In addition to its well-known role in transepithelial sodium transport across ductal membranes, growing evidence suggests involvement of ENaC in epithelial maturation and regeneration homeostasis via functions that involve the sensing of the extracellular environment.[13,14]

We hypothesized that ENaC plays a critical role in the physiology and pathophysiology of the MG. To test this hypothesis, the effects of *βENaC* deletion in the gene expression, morphology, and function of mouse MG and ocular surface epithelia were investigated. A conditional MG *βENaC* knockout mouse, with deletion of *βENaC* (*Scnn1b*) in MG acinar and ductal cells, but not conjunctiva and cornea, was generated by crossing Sonic Hedgehog (*Shh*)−Cre mice with floxed *βENaC* mice. Because of the female-dominant prevalence of dry eye and sex steroid hormone regulation of human MG function, male and female mice were separated for comparative phenotypic studies.[2,15] Primary mouse MG cell cultures were generated to test the role of ENaC in MG cell proliferation.

## Materials and Methods

### Animals

Frozen embryos of floxed *βENaC* mice (C57/B6 background) were purchased from the European Mouse Mutant Archive (Neuherberg, Germany) and resuscitated at the Animal Mouse Model Core at University of North Carolina at Chapel Hill.[16] *Shh*-Cre mice (C57/B6 background) and B6;129S6-Gt(ROSA)-26Sor$^{tm1(CAG-tdTomato,-EGFP)Ees}$/J were purchased from the Jackson Laboratory (Bar Harbor, ME) and crossbred to check for Shh localization in ocular tissues. Exon 2 floxed *βENaC* mice were crossed to *Shh*-Cre mice to specifically delete βENaC expression in MG tissues. The conditional *βENaC* knockout mice were homozygous for the floxed *βENaC* and heterozygous for *Cre* and *Shh* (*βENaC*$^{fl/fl}$;Shh-Cre$^{+/−}$). Floxed *βENaC* mice were used as littermate controls. Genotyping of offspring mice was performed by PCR with the following primers: for Cre mutant, 5′-GGGACAGCTCACAAGTCCTC-3′ (forward) and 5′-GGTGCGCTCCTGGACGTA-3′ (reverse) (product size, 350 bp); for wild-type *Shh* gene, 5′-GGGACAG-CTCACAAGTCCTC-3′ (forward) and 5′-CTCGGCTACGT-TGGGAATAA-3′ (reverse) (product size, 200 bp); and for *βENaC*, 5′-CACTCAGGCACATGATAGACAGG-3′ (forward) and 5′-CTGCTCTGGGATTACAGG-3′ (reverse) (product sizes, 430 bp from the *βENaC*$^{flox}$ allele and 280 bp from the wild-type *βENaC* gene).[16] Animals were studied in compliance with the Association for Research in Vision and Ophthalmology statement for the Use of Animals in Ophthalmic and Vision Research, and protocols were approved by the Institutional Animal Care and Use Committee of University of North Carolina at Chapel Hill.

### Measurement of Aqueous Tear Production

Tear production was measured with the phenol red thread test using Zone-Quick cotton threads (Oasis Medical Inc., Glendora, CA). Briefly, animals were anesthetized by i.p. injection of 1.25% tribromoethanol (Avertin; Sigma-Aldrich, St. Louis, MO). Two minutes after the injection, phenol red−stained threads were gently inserted into the lateral canthus of anesthetized mouse for 20 seconds.[17] The wetting distance of the thread was measured in millimeters to quantitate tear production.

### Mass Spectrometric Analysis of Tears

Tears collected by phenol red threads were eluted in 200 μL distilled water, vortex mixed, and frozen for subsequent analysis. Liquid chromatography−tandem mass spectrometry was performed using a previously described method.[18] Briefly, 15 μL of an internal standard solution of isotopically labeled purines, urea, amino acids, and sialic acid was added to 100 μL of diluted tear samples, and samples were lyophilized to dryness overnight and resuspended in 15 μL high-performance liquid chromatography grade water. Resuspended samples (5 μL) were injected into a liquid chromatography−tandem mass spectrometry system consisting of an Acquity solvent manager and a TSQ Quantum UltraTriple Quadrupole Mass Spectrometer (Thermo Fisher Scientific, San Jose, CA). An Atlantis T3 C18, 1.8-μm column (Waters, Milford, MA) was operated with a gradient of 5% methanol−0.1% formic acid to 80% methanol−0.1% formic acid over 4 minutes. Metabolites were detected in positive-mode electrospray ionization liquid chromatography−tandem mass spectrometry by selected reaction monitoring of the appropriate mass/charge ratio transitions.[18]

### Inductively Coupled Plasma Optical Emission Spectrometry

Concentrations of sodium in diluted tear samples were measured using inductively coupled plasma optical emission spectrometry (Optima 4300 DV; PerkinElmer, Norwalk, CT), as previously reported.[19] Briefly, 60 μL aliquots of diluted tear samples were added to 3 mL of deionized

**Table 1** Oligonucleotide Primers for Real-Time RT-PCR

| Gene | Sequence | | Accession no. | Product size, bp |
|---|---|---|---|---|
| | Forward | Reverse | | |
| *αENaC* | 5′-TGTGGAGACCTCCATCAGTATG-3′ | 5′-CCTTGGGCTTAGGGTAGAAGAT-3′ | NM_011324.2 | 206 |
| *βENaC* | 5′-CAGACCTACCTGAGCTGGGA-3′ | 5′-CCTTGAGCAAGTGCTTGACCT-3′ | NM_011325.2 | 127 |
| *γENaC* | 5′-GCTTCTGAGAAATGGTTGCTG-3′ | 5′-CGAGCTGTCCACCAAAGTTAG-3′ | NM_011326.2 | 184 |
| *Mmp9* | 5′-GAAGCGGACATTGTCATCCA-3′ | 5′-AAATGGGCATCTCCCTGAAC-3′ | NM_13599.4 | 125 |
| *IL1α* | 5′-CTGCAGTCCATAACCCATGA-3′ | 5′-TGACAAACTTCTGCCTGACG-3′ | NM_010554.4 | 115 |
| *IL1β* | 5′-CATGGAATCCGTGTCTTCCTA-3′ | 5′-AGAATGTGCCATGGTTTCTTG-3′ | NM_008361.3 | 172 |
| *KC* | 5′-GCTGGGATTCACCTCAAGAA-3′ | 5′-AAGGGAGCTTCAGGGTCAAG-3′ | NM_008176.3 | 184 |
| *IL13* | 5′-AACATCACACAAGACCAGACTC-3′ | 5′-GGTTACAGAGGCCATGCAATA-3′ | NM_008355.3 | 160 |
| *Ym1* | 5′-AACATCACACAAGACCAGACTC-3′ | 5′-GGTTACAGAGGCCATGCAATA-3′ | NM_009892.3 | 131 |
| *Muc4* | 5′-CAGTTTGATGAGGAGCAGGAG-3′ | 5′-AGAAACCACTGAACCGTGATG-3′ | NM_080457.3 | 193 |
| *Muc5ac* | 5′-CAGCCGAGAGGAGGGTTTGATCT-3′ | 5′-AGTCTCTCTCCGCTCCTCTCAAT-3′ | NM_010844.1 | 353 |
| *Muc5b* | 5′-GGATAACTGTACCTCCGTGCTC-3′ | 5′-CGGTCACACCATTCTTACTGAA-3′ | NM_028801.2 | 248 |
| *Ki-67* | 5′-CCAGCTGCCTGTAGTGTCAA-3′ | 5′-CTCCATGTCTCAGCCTCACA-3′ | NM_001081117.2 | 140 |
| *Gapdh* | 5′-GGAGAAACCTGCCAAGTATGA-3′ | 5′-TCCTCAGTGTAGCCCAAGA-3′ | NC_000072.6 | 90 |

The NCBI Nucleotide Database is available at *http://www.ncbi.nlm.nih.gov/nuccore* (last accessed September 28, 2017).

water, and this solution was assayed. Quality assurance checks were obtained using a second multielement standard (SPEX CertiPrep, Metuchen, NJ). Specific wavelengths for sodium were 588.995 and 589.592 nm. A multielement standard (VHG Labs, Manchester, NH) was used for the calibration curve.

## Real-Time RT-PCR Analysis

Meibomian gland and conjunctival tissues were isolated under a dissecting microscope (Olympus Co, Tokyo, Japan), homogenized with a Minilys homogenizer (Bertin Technologies, Ampere Montigny-le-Bretonneux, France), and extracted for total RNA with Direct-zol RNA MiniPrep with TRI Reagent (Genesee, Irvine, CA), in accordance with the manufacturer's instructions. cDNAs were synthesized by reverse transcribing RNA using Verso cDNA synthesis kits (Thermo Fisher Scientific, Waltham, MA). SYBR Green real-time PCR assays were performed to analyze the relative quantitative expression of selected genes of interest with primers shown in Table 1. Expression levels were normalized to the expression of glyceraldehyde-3-phosphate dehydrogenase mRNA. The βENaC primer pair flanking the exon 2 of βENaC was designed to yield a PCR product of 127 bp from the control, but not the mutant, transcript.

## Histopathology of Meibomian Gland and Ocular Surface Epithelia

Mouse whole eyeballs and eyelids were harvested and fixed with 10% neutral-buffered formalin overnight at room temperature and processed for paraffin embedding. For the whole eyeball blocks, serial sections (8 μm thick) were cut along the sagittal axis from the center of the pupil to the retina to provide sections of the complete conjunctiva. Coronal sections of eyelids were also cut to view the morphology of MG, including ducts and acini. Sections were stained with hematoxylin and eosin.

## Scanning Electron Microscopy

For scanning electron microscopy, eyes were excised and fixed in 4% formalin before being processed, as previously reported.[20] All specimens were then impregnated with 2.5% tannic acid for 2 days. Counterfixation in 2% $OsO_4$ for 4 hours was followed by dehydration in ethanol and drying in a critical point dryer (Leica EM CPD 300; Leica Microsystems, Wetzlar, Germany). The preparations were coated with gold and examined with a scanning electron microscope (Jeol JSM-IT 300; JEOL, Tokyo, Japan).[20]

## Transmission Electron Microscopy

MG tissues were excised and processed for transmission electron microscopy, according to a protocol reported previously.[12] In brief, tissues were fixed in Ito fixative (2.5% glutaraldehyde, 2.5% paraformaldehyde, and 0.3% picric acid dissolved in phosphate-buffered saline, pH 7.3) and embedded in Epoxy embedding medium (Sigma-Aldrich). Semithin sagittal sections (1 μm thick) were cut with a microtome (Ultracut E; Reichert Jung, Vienna, Austria) and subsequently stained with toluidine blue. Sections were viewed with an epifluorescence microscope (Aristoplan; Ernst Leitz, Wetzlar, Germany) and imaged (DC 500 camera; Leica Microsystems). Ultrathin sections were stained with uranyl acetate and lead citrate and viewed with a transmission electron microscope (EM109; Carl Zeiss Meditec GmbH, Oberkochen, Germany).[21]

## Immunohistochemistry

Tissue sections were deparaffinized, hydrated, and subjected to antigen retrieval by microwave subboiling for 10 minutes

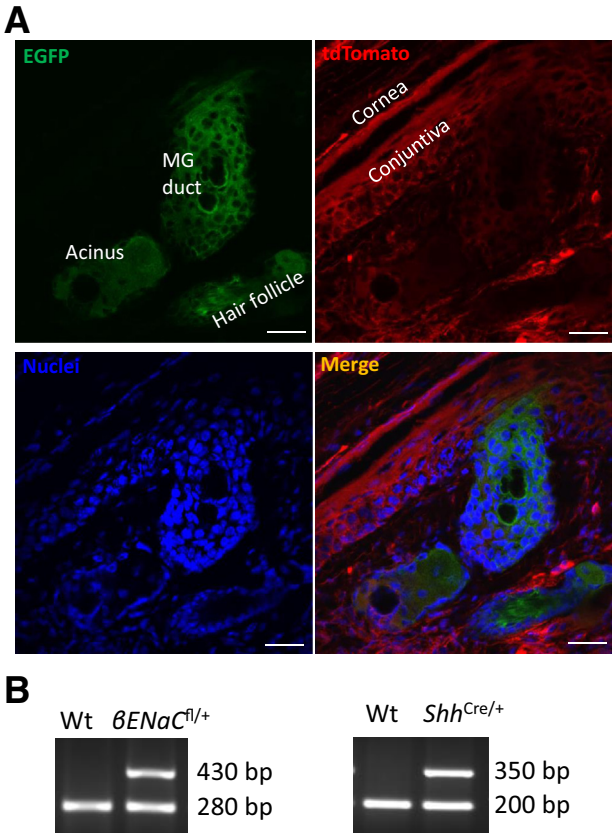


**Figure 1** Sonic Hedgehog (Shh) distribution in the ocular tissues of Gt(ROSA)26Sor$^{(CAG\text{-}tdTomato,\text{-}EGFP)}$;*Shh*-Cre$^{+/-}$ mice. **A:** Shh expression, as indicated by the EGFP signal, is present exclusively in MG acini and ducts [enhanced green fluorescent protein (EGFP)] and is absent in cornea or conjunctiva (tdTomato). **B:** Genotyping of *βENaC*$^{fl/fl}$;*Shh*-Cre$^{+/-}$ mice by RT-PCR. The *βENaC*$^{flox}$ allele and wild-type (Wt) *βENaC* gene produce products of 430 and 280 bp, respectively. The *Shh*$^{cre}$ mutant and normal *Shh* gene produce products of 350 and 200 bp, respectively. Scale bars = 25 μm. Original magnification, ×40.

in 10 mmol/L citrate acid (pH 6.0).[12] Sections were then treated with 30% hydrogen peroxide for 30 minutes, blocked with 4% normal serum and 0.1% Triton X-100 (Sigma-Aldrich) in phosphate-buffered saline at room temperature for 1 hour, and incubated with primary antibodies diluted in blocking buffer at 4°C overnight. The primary antibodies are described in Table 1. Normal IgG from Vector Laboratories (Burlingame, CA) was used as a negative control. Slides were incubated with biotinylated secondary antibodies for 30 minutes to 1 hour at room temperature, followed by 30 minutes of incubation with Vector Elite ABC reagent (Vector Laboratories). The immunostaining signal was developed by nickel-diaminobenzidine (Sigma-Aldrich), followed by incubation with Tris-cobalt and counterstaining with Nuclear Fast Red. Finally, the sections were serially dehydrated, mounted with DPX mountant for histology (Sigma-Aldrich), and visualized with light microscopy (Nikon, Tokyo, Japan). The immunostaining intensity of Ki-67 was measured by ImageJ version 1.47 (NIH, Bethesda, MD; *http://imagej.nih.gov/ij*).[22] Briefly, the ratio of positively stained areas of cells/the perimeter of the selected MG acini and conjunctival epithelia was calculated for comparison.

## Multiplex Assays of IL-1α and Keratinocyte Chemoattractant (KC) Levels in Conjunctival Tissues

Conjunctival tissues were dissected and homogenized with a Minilys homogenizer in phosphate-buffered saline and protease inhibitors (Invitrogen Life Technologies) and extracted for protein with radioimmunoprecipitation assay buffer at 4°C overnight. After centrifugation, the supernatants were collected and stored at −80°C until later analysis. Cytokines were analyzed with Milliplex Map Mouse Cytokine/Chemokine Magnetic Bead Panel-Immunology Multiplex Assay (EMD Millipore, Billerica, MA) and a Luminex 100 TM system (Bio-Rad Laboratories, Hercules, CA). Beads were prepared according to the manufacturer's instructions. Measurements were made in duplicate for each sample. Standard curves were generated by using the reference cytokine concentrations supplied by the manufacturer.

## Mouse Meibomian Gland Cell Co-Culture with 3T3 Feeder Cells and a ρ Kinase Inhibitor

Primary mouse MG cells were isolated similar to a protocol described previously.[12] Briefly, tissues harvested from 2- to 3-month−old female and male, control and *βENaC* MG knockout (KO) mice were digested with 2 mg/mL collagenase (Sigma-Aldrich) and 0.2 mg/mL dispase II (Roche Applied Science, Indianapolis, IN) at 37°C for 2 hours. Cell suspensions were dissociated into single cells by Accutase (Innovative Cell Technologies, Inc., San Diego, CA) treatment for 25 minutes. Isolated MG cells were cocultivated with mitomycin C−treated 3T3-Swiss Albino fibroblasts in F medium [Dulbecco's modified Eagle's medium/Nutrient Mixture F-12, 3:1 (v/v), supplemented with 5% fetal bovine serum, 0.1 μg/mL hydrocortisone (Sigma-Aldrich), 5 μg/mL insulin (Sigma-Aldrich), 8.4 ng/mL cholera toxin (Sigma-Aldrich), 10 ng/mL epidermal growth factor (Invitrogen Life Technologies), 0.25 μg/mL amphotericin B (Sigma-Aldrich), 10 μg/mL gentamicin (Sigma-Aldrich), and 10 μmol/L Y-27632 (ρ kinase inhibitor; Enzo Life Sciences, Farmingdale, NY)]. All cells were maintained at 37°C in a humidified incubator with 95% $O_2$ and 5% $CO_2$. During subculture, 3T3 feeder cells and MG epithelial cells were separated by their differential time requirements for Accutase digestion.

## Cell Proliferation Assay

Cell proliferation was measured with the Premix WST-1 Cell Proliferation Assay System (Takara Bio USA, Mountain View, CA), according to the manufacturer's protocol. The WST-1 test is based on the cleavage of the tetrazolium salt to formazan by mitochondrial dehydrogenase enzymes. Passaged mouse MG cells were seeded onto 96-well plates

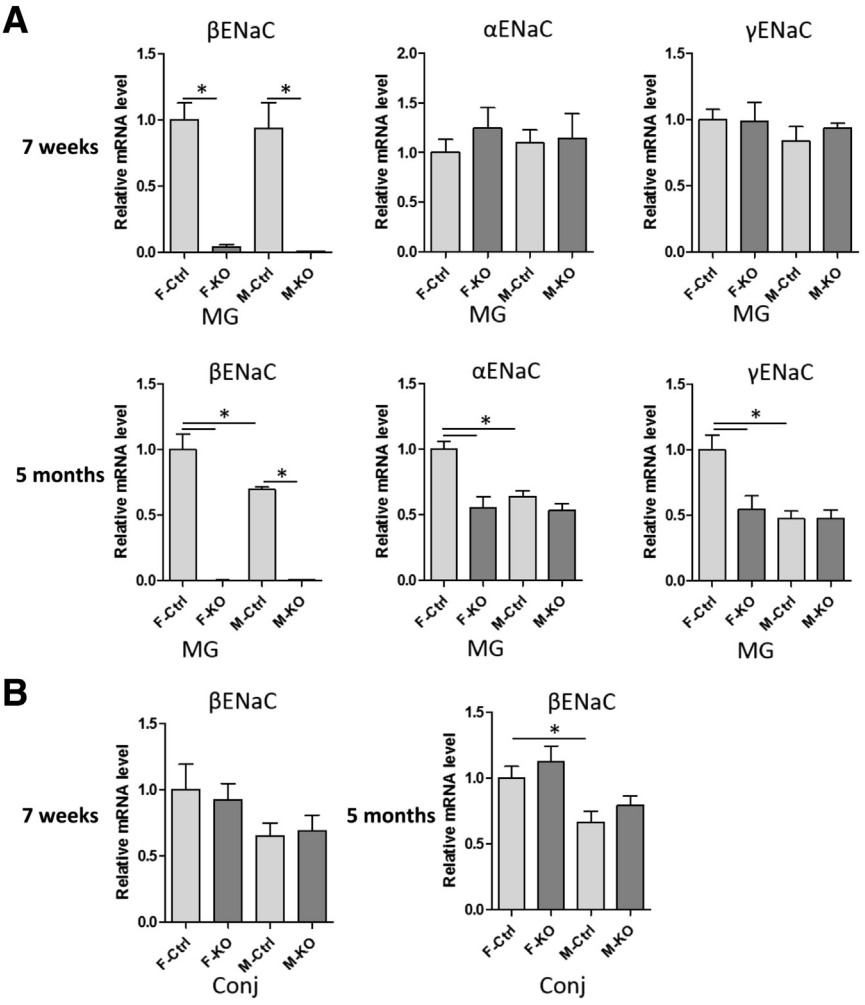


**Figure 2** Quantitative analysis of α, β, and γ ENaC mRNA expression in MG and conjunctival tissues of control and *βENaC* MG KO mice. **A: Top row:** βENaC mRNA expression is deleted in MG tissues of both female (F) and male (M) 7-week−old *βENaC* MG KO mice, and the expression of α and γ ENaC mRNA expression is unchanged in MG. **Bottom row:** The βENaC mRNA deletion in MG tissues remains stable in 5-month−old *βENaC* MG KO mice. However, there are lower levels of α and γ ENaC mRNA in female, but not male, *βENaC* MG KO than control (Ctrl) mice. **B:** Expression of βENaC is not different in conjunctival (Conj) tissues of *βENaC* MG KO versus control mice at 7 weeks and 5 months. $*P < 0.05$.

and treated with 10 μmol/L benzamil (an ENaC inhibitor) or vehicle control for 2 hours. The WST-1 reagent was applied for 1.5 hours at 37°C, and the plate was measured at 450 and 630 nm by a plate reader (Victor 3V Multilable Countermodel 1420; PerkinElmer, Waltham, MA).

### Statistical Analysis

Data are described as means ± SEM. Statistical tests were performed using GraphPad Prism software version 5.0 (GraphPad Software, San Diego, CA). Differences among each group were analyzed by analyses of variance. Visible severe corneal defects was coded as follows: 1, yes; and 0, no. The binomial response variable was analyzed by logistic regression, with sex and genotype/strain as independent variables, using the generalized linear models function in R (R Foundation for Statistical Computing, Vienna, Austria). The estimated odds ratio and 95% CIs from generalized linear model fittings were plotted. An unpaired *t*-test was used to compare the Ki-67 immunostaining intensity between two groups. $P < 0.05$ was considered significant.

## Results

### Generation of Conditional *βENaC* Knockout Mouse Model with Cre-Loxp System

βENaC is localized to the peripheral area of the MG acinus, but not ducts, in rat.[12] The expression of Shh in the murine eyes was tested from analyses of Gt(ROSA)26Sor$^{(CAG\text{-}tdTomato,\text{-}EGFP)}$/*Shh* Cre$^{+/-}$ mice (Figure 1A). Shh was exclusively expressed in MG acini and ducts and was not expressed in conjunctiva or cornea. Accordingly, *Shh* Cre$^{+/-}$ mice were crossed with floxed *βENaC* (*βENaC*$^{fl/fl}$) mice to study the effects of MG *βENaC* deletion on MG health and possible downstream effects on the ocular surface (Figure 1B).

More than 95% of βENaC mRNA expression was deleted in MG tissues of conditional *βENaC* MG KO mice compared with control mice (Figure 2A). The deletion was stable in both 7-week−old and 5-month−old mice. In contrast, βENaC mRNA expression in conjunctival tissues was not altered by the Shh-Cre construct (Figure 2B). The expression of α- and γ-ENaC in the *βENaC* MG KO mice

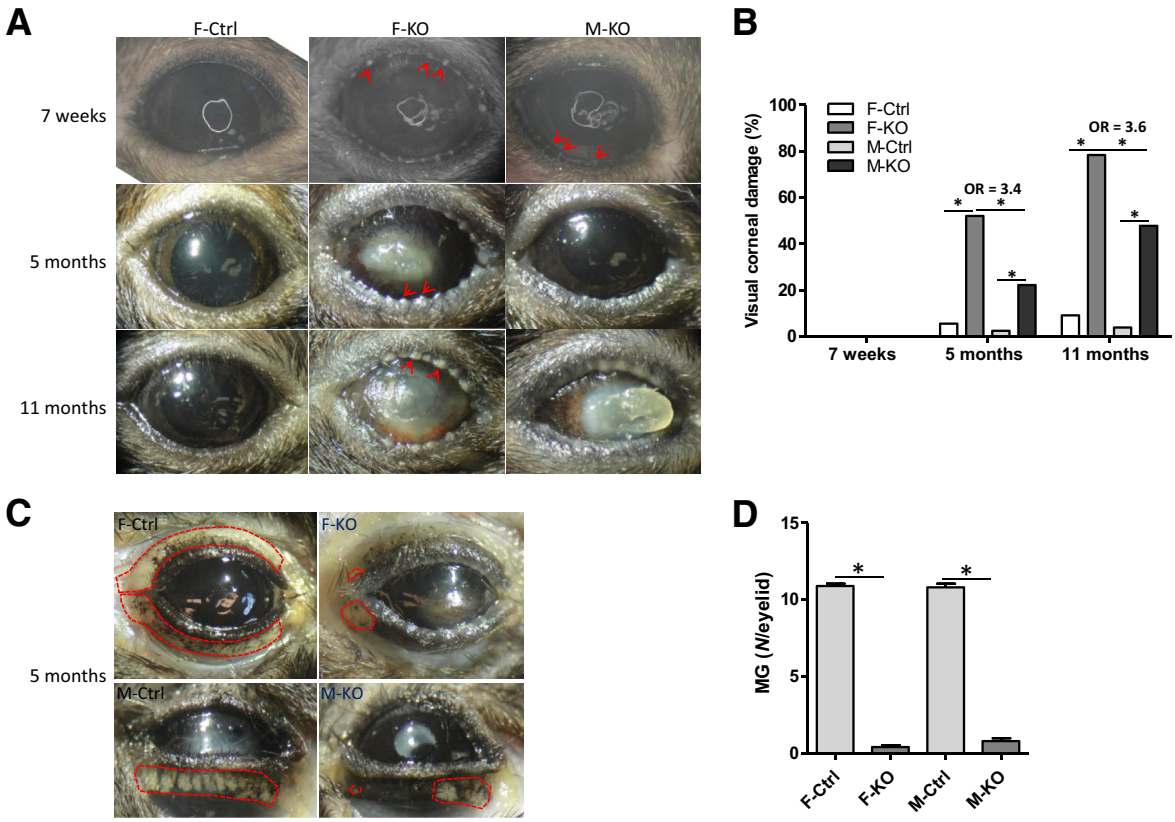


**Figure 3** Phenotypic changes of the ocular surface associated with *βENaC* deletion in MG at 7 weeks (7w), 5 months (5m), and 11 months (11m) of age. **A:** There is MG orifice obstruction with white secretions in *βENaC* MG KO mice as early as 7 weeks of life. **Red arrows** indicate obstructed MG orifices. In 5- and 11-month–old mice, there are prominent MG obstructions, swollen eyelid margins, and striking corneal pathologies, including corneal opacification, ulceration, perforation, neovascularization, and ectasia. **B:** The incidence of visible severe corneal defects in 5-month–old female (F; 52.0%) is higher than in male (M; 22.2%) *βENaC* MG KO mice [$P = 0.044$; odds ratio (OR), 3.4; 95% CI, 1.1–12.3]. In the 11-month–old groups, the percentage of mice exhibiting visible severe corneal abnormalities is 78.4% and 47.8% in female and male *βENaC* MG KO mice, respectively. The incidence of visible defects in female *βENaC* MG KO mice is significantly higher than that in male *βENaC* MG KO mice ($P = 0.014$; OR, 3.6; 95% CI, 1.3–10.7). **C:** Gross dissection of eyelids reveals widespread MG atrophy in 5-month–old *βENaC* MG KO mice, irrespective of corneal abnormalities. **Red dashed lines** outline the MG region. **D:** Quantitative comparison of numbers of MG in eyelids of *βENaC* MG KO and control (Ctrl) mice. $^*P < 0.05$.

was not affected at 7 weeks but was decreased at 5 months in female, but not male, mice.

To test for sex-related differences in ENaC gene expression, ENaC expression of female and male control mice was compared (Figure 2A). Female mice exhibited similar expression levels of α-, β-, and γ-ENaC mRNAs as male mice at 7 weeks. In contrast, female mice exhibited significantly higher expression of all ENaC subunits than males at 5 months.

## Deletion of *βENaC* in MG Produces Pathognomonic Phenotype of MGD in a Sex-Dependent Manner

*βENaC* MG KO mice exhibited a striking ocular phenotype, with white secretions obstructing the MG orifices as early as 7 weeks of life (Figure 3A). Notably, an ocular surface phenotype was more penetrant in female *βENaC* MG KO than male mice at all ages. In addition to the prominent MG obstructive phenotype and swollen eyelid margins, there were dramatic corneal pathologies, including corneal opacification, ulceration, perforation, neovascularization, and ectasia, in older mice (Figure 3A). The incidences of these visible severe corneal defects in 5-month–old female ($N = 25$) and male ($N = 18$) *βENaC* MG KO mice were 52.0% and 22.2%, respectively (Figure 3B). There was a significant difference in visible pathology between female and male *βENaC* MG KO mice ($P = 0.044$; odds ratio, 3.4; 95% CI, 1.1–12.3). In the 11-month–old groups, the percentages of mice exhibiting visible severe corneal abnormalities were 78.4% and 47.8% for female ($N = 37$) and male ($N = 23$) *βENaC* MG KO mice, respectively (Figure 3B). The incidence of visible pathology in female *βENaC* MG KO mice was significantly higher than in male *βENaC* MG KO mice ($P = 0.014$; odds ratio, 3.6; 95% CI, 1.3–10.7). Ocular surfaces of 11-month–old *βENaC* MG KO mice are shown in Supplemental Figure S1.

As revealed by the gross dissections of the eyelid, deletion of *βENaC* in MG resulted in widespread MG atrophy in 5-month–old *βENaC* MG KO mice, regardless of the presence of severe corneal abnormalities (Figure 3C). There were 9 to 12 MGs in the upper and lower eyelids in control mice. In most *βENaC* MG KO mice, nearly all glands were

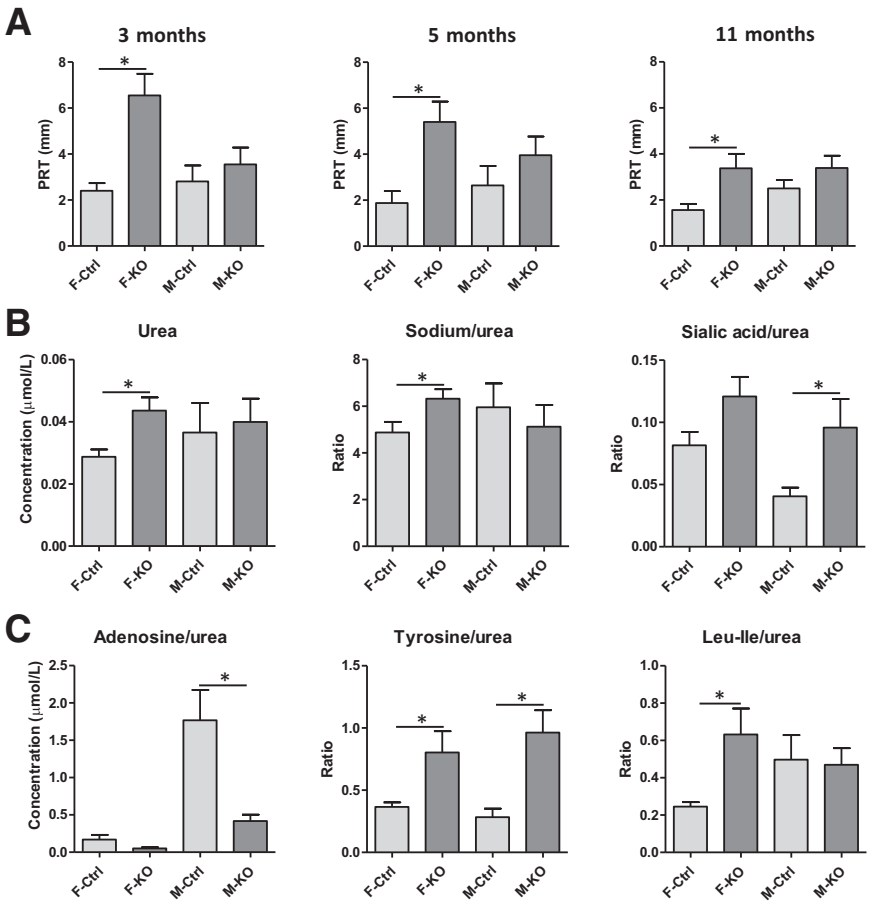


**Figure 4** Tear production measurement and tear component analysis. **A:** The tear volume measured by the phenol red thread (PRT) test is consistently higher in 3-, 5-, and 11-month—old female (F) *βENaC* KO mice than control (Ctrl) mice. Similar trends, but no significant differences, are observed in male (M) mice. **B:** Analysis of urea and sodium/urea and sialic acid/urea ratios in female and male *βENaC* MG KO and control mice. **C:** Liquid chromatography—tandem mass spectrometry analyses of adenosine, tyrosine, and leucine/isoleucine to urea ratios in control and *βENaC* MG KO mice. $^*P < 0.05$.

lost by 5 months, except for a single most lateral MG gland that remained in some *βENaC* MG KO mice (Figure 3, C and D).

## Evaluation of Ultrastructure of Meibomian Gland

To evaluate the ultrastructure of the MG, remaining MG tissues were collected from three 5- and 11-month—old male *βENaC* MG KO and control mice for transmission electron microcopy studies (Supplemental Figure S2). Control mice analyzed revealed normal basal, differentiating, mature, and hypermature meibocytes. The cytoplasm of basal meibocytes was filled with vacuoles containing lipids. Differentiating meibocytes showed changes from more rounded vacuoles to a more vermicular form. Mature and hypermature meibocytes demonstrated more and more condensation of the cells, including dense bodies with a crystalline appearance. This feature was accompanied by nuclear condensation and pycnosis consistent with meibocyte differentiation. Finally, the crystals marked the appearance of dense masses in hypermature meibocytes. No differences were ultrastructurally visible between control MG and the remaining MG in *βENaC* MG KO mice as a function of age.

## *βENaC* MG KO Mice Exhibit Evidence for Hyperosmolar Tears and Increased Tear Production as a Compensatory Response to Meibomian Gland Dysfunction

The tear volume measured by the phenol red thread test was higher in female *βENaC* MG KO mice than in control mice (Figure 4A). This difference was observed consistently in 3-, 5-, and 11-month—old female KO mice. Similar trends were observed in male mice. Mass spectrometric analysis of tears demonstrated higher levels of urea in diluted tear samples of 5-month—old *βENaC* MG KO mice, consistent with increased volume measured by the phenol thread test (Figure 4B).

Utilizing urea as the dilution marker, evidence for hyperconcentration of small solutes (eg, ions) and large molecules (eg, mucins) in the tear film was observed. For example, the ratio of sodium/urea was increased in female mice, suggesting the tears of female *βENaC* MG KO mice were hypertonic (Figure 4B). Sialic acid has been used in our mass spectrometry assays as a marker of mucin concentration.[18] The increased sialic acid/urea rates in male *βENaC* MG KO mice suggest mucins were concentrated in tears as well (Figure 4B).

Markers of inflammation were also detected in tears by mass spectrometry, and these markers were given as ratios to urea. Decreased levels of adenosine were detected in male

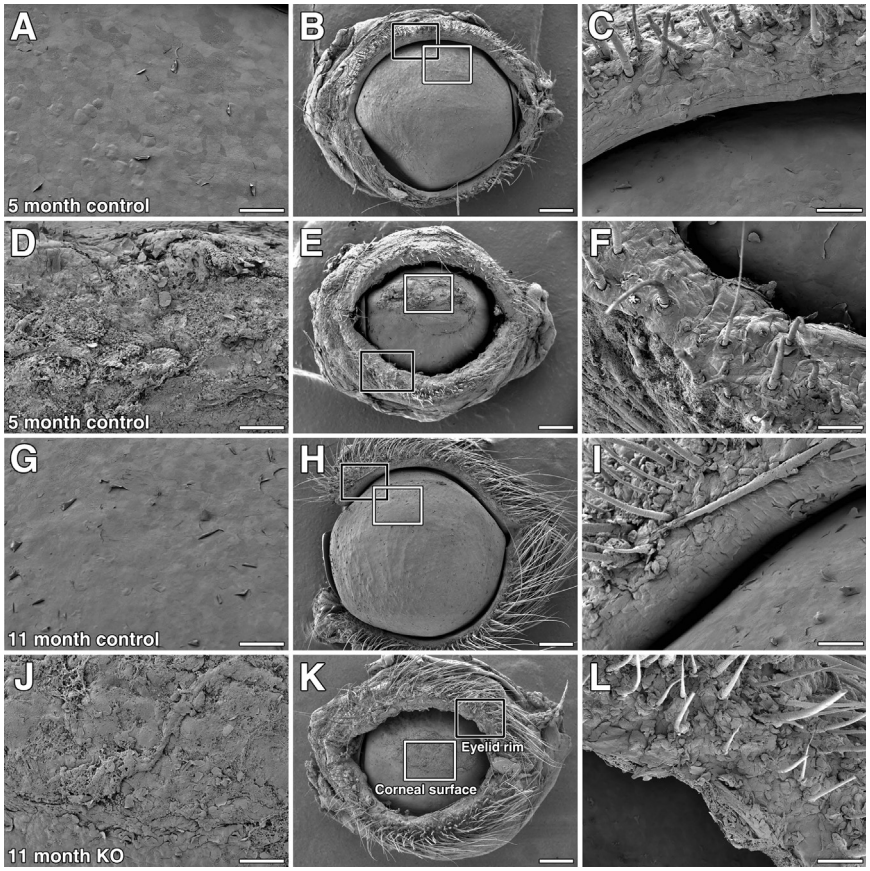


**Figure 5** Scanning electron micrographs of the corneal surface (**left** and **middle columns**) and eyelid rim (**middle** and **right columns**) of 5- and 11-month—old male *βENaC* MG KO and control mice. **Middle column** show whole eyes with surrounding eyelid apparatus. **Left column** display magnifications of the corneal surface from the relevant image in the **middle column** (**white boxed areas**). **Right column** display magnifications of the eyelid rim from the relevant image in the **middle column** (**black boxed areas**). **A**, **B**, **G**, and **H:** Control mice at 5 and 11 months have a smooth ocular surface consisting of noncornifying squamous epithelium. **D**, **E**, **J**, and **K:** *βENaC* MG KO mice at 5 and 11 months exhibit desiccation (dry eye disease) at the ocular surface with cornification of the central corneal surface. **B**, **C**, **E**, **F**, **H**, **I**, **K**, and **L:** Control mice at 5 and 11 months have a smooth and clear eyelid rim (**B**, **C**, **H**, and **I**), whereas *βENaC* MG KO mice at 5 and 11 months have an irregular eyelid rim with epithelial stratification and closure of meibomian gland orifices (**E**, **F**, **K**, and **L**). No differences are obvious between 5- and 11-month—old KO mice. Scale bars: 100 μm (**A**, **C**, **D**, **F**, **G**, **I**, **J**, and **L**); 500 μm (**B**, **E**, **H**, and **K**).

*βENaC* MG KO compared with control mice (Figure 4C). The reduced adenosine levels may reflect increased metabolism of adenosine by inflammation-induced release of adenosine deaminase, but higher xanthine, hypoxanthine, and uric acid levels were only observed in female *βENaC* MG KO mice (Supplemental Figure S3). In female *βENaC* MG KO mice, tyrosine, leucine/isoleucine, ornithine, and methionine levels in tear fluid were increased (Figure 4C

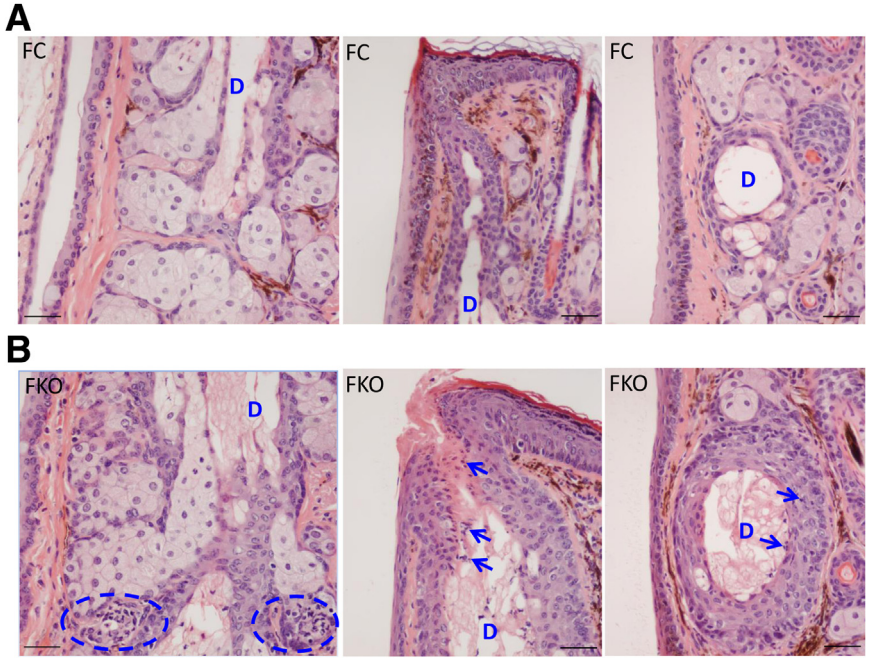


**Figure 6** MG histology of 3-month—old female control (FC; **A**) and *βENaC* MG KO (FKO; **B**) mice. MG ducts (D) are shown. Inflammatory cell infiltration is observed in both MG acini and ducts of *βENaC* MG KO mice, with duct enlargement and ductal epithelial cell hyperstratification. **Dashed ovals** outline a cluster of inflammatory cell infiltration in the MG. **Arrows** indicate the presence of inflammatory cells among MG orifice and ductal epithelial cells. Scale bars = 50 μm (**A** and **B**). Original magnification, ×20 (**A** and **B**).

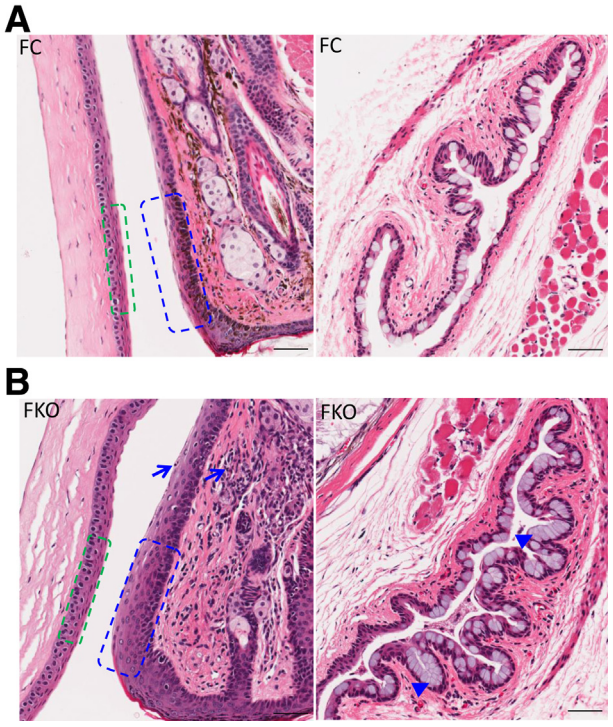


**Figure 7** Ocular surface epitheliopathy associated with *βENaC* deletion in MG. **A:** Ocular surface histology of 5-month–old female control (FC) mouse. **Left panel:** Eyelid wiper and corneal regions. **Right panel:** Fornical conjunctival region. **B:** Comparable regions from 5-month–old female *βENaC* MG KO (FKO) mouse. **Green dashed lines** outline the corneal epithelia. **Blue dashed lines** outline the palpebral conjunctiva. In the female *βENaC* MG KO mouse, hyperstratification in both the corneal and conjunctival epithelia, particularly in the eyelid wiper area, is observed. Inflammatory cells, as indicated by **arrows**, infiltrate the conjunctival epithelia and connective tissues. In addition, there are large clusters of goblet cells, as indicated by **arrowheads**, in the fornical conjunctiva. Scale bars = 50 μm (**A** and **B**). Original magnification, ×20 (**A** and **B**).

and Supplemental Figure S3). In male *βENaC* MG KO mice, significantly higher levels of phenylalanine and tyrosine in tear fluids were observed compared with control mice (Figure 4C and Supplemental Figure S3). The higher levels of free amino acids may represent tear fluid proteolytic activities. The levels of AMP, inosine, proline, taurine, nicotinamide, methylthioamphetamine, and glutathione disulfide were similar in all groups (data not shown).

## Scanning Electron Microscopy

Scanning electron micrographs revealed irregular ocular surfaces and eyelid rims in both 5- and 11-month–old male *βENaC* MG KO mice (Figure 5). *βENaC* MG KO mice exhibited roughened areas on the ocular surface with cornification of the central corneal surface. No differences were detected between 5- and 11-month–old *βENaC* MG KO mice. Control mice at similar ages exhibited smooth eyelid margins and ocular surfaces consisting of non-cornifying squamous epithelium.

## Histopathology of the Ocular Surface Caused by Loss of βENaC in MG

Histologically, mild inflammatory cell infiltrations were observed in both MG acini and ducts of female *βENaC* MG KO mice, with duct enlargement and ductal epithelial cell hyperstratification also visible (Figure 6). These histopathological changes of MG were also apparent at 3 months of age in male *βENaC* MG KO mice (Supplemental Figure S4). The dysfunction of MG resulting from the progressive MG pathologies produced a corneal and conjunctival epitheliopathy in older mice. For example, in 5-month–old *βENaC* MG KO mice, histological studies revealed hyperstratification in both corneal and conjunctival epithelia, particularly in the eyelid wiper area (Figure 7 and Supplemental Figure S5). Inflammatory cells infiltrated the conjunctival epithelia and connective tissues. In addition, there was goblet cell hyperplasia in the fornical conjunctiva of *βENaC* MG KO mice (Figure 7 and Supplemental Figure S5). The goblet cells became larger and fused into large clusters, which was rarely seen in the control mice.

The histopathological changes of the ocular surface of 11-month–old *βENaC* MG KO mice were striking. Most of MG acini were atrophied, with hyperkeratinized and hyperstratified ductal epithelial cells and persistent leukocytic infiltration. There was widespread corneal epithelial hyperkeratinization, hyperstratification, and neovascularization (Figure 8 and Supplemental Figure S6). The corneal epithelium resembled skin epidermis. There was prominent cornification and hyperstratification in the palpebral conjunctival epithelial cells, together with goblet cell hyperplasia and hyperstratification of fornical conjunctival epithelia.

## Inflammation of MG and Conjunctiva Induced by *βENaC* Deletion

Consistent with histological observations of inflammatory cell infiltration in MG and conjunctival tissues, cytokine mRNA expression patterns consistent with inflammation were observed in both MG and conjunctival tissues from *βENaC* MG KO mice. Il-1β, Kc (a functional homologue of human IL-8), Il-13, Beta-N-acetylhexosaminidase Ym1 (Ym)1 (a monocyte marker), and matrix metalloproteinase 9 mRNA expression levels were significantly increased in the MG tissues of 5-month–old female *βENaC* MG KO mice compared with control mice (Figure 9A). In male *βENaC* MG KO mice, similar trends were observed, with statistical differences in Il-1β, Kc, Il-13, and Ym1 between *βENaC* MG KO and control mice.

In conjunctival tissues, Kc and Il-13 mRNA levels were increased in both female and male *βENaC* MG KO mice compared with control mice (Figure 9B). The elevated Il-13 levels were consistent with fornical goblet cell hyperplasia and elevations in Muc4 and Muc5ac (Figure 9, B and C).

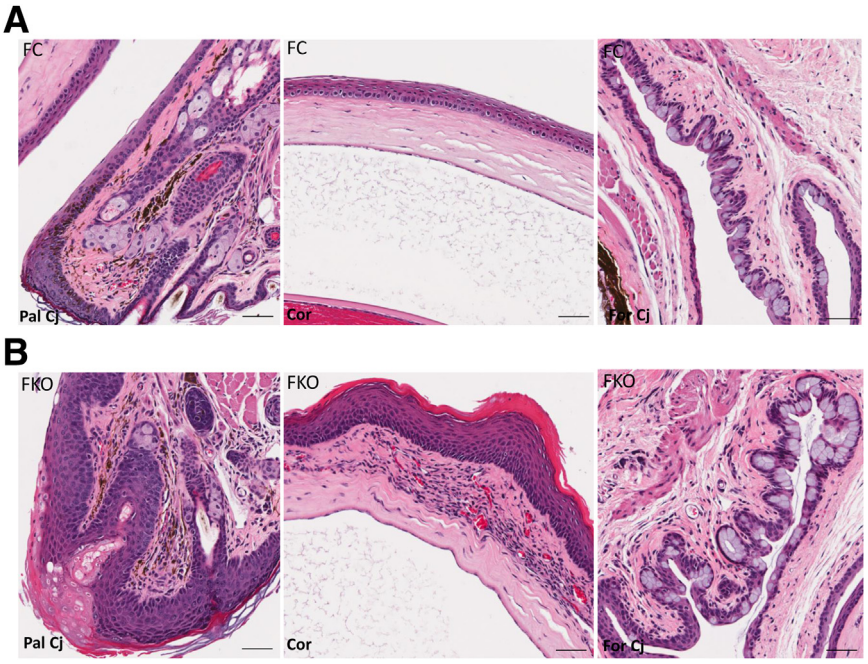


**Figure 8** The histopathological changes of ocular surface tissues of 11-month—old mice. **A:** Histology of female control (FC) mouse. **Left panel:** Eyelid skin, mucocutaneous junction, including eyelid wiper, palpebral conjunctiva (Pal Cj), and MG. **Middle panel:** The cornea (Cor). **Right panel:** Bulbar and fornical conjunctiva (For Cj). **B:** Histology of 11-month—old female *βENaC* MG KO (FKO) mouse. **Left panel:** Hyperkeratinized and hyperstratified MG orifice epithelial cells and palpebral conjunctival epithelial cells. **Middle panel:** Widespread corneal epithelial hyperkeratinization, hyperstratification, and neovascularization. The corneal epithelia resemble skin epidermis. **Right panel:** There is prominent goblet cell hyperplasia and hyperstratification of fornical conjunctival epithelia. Scale bars = 50 μm (**A** and **B**). Original magnification, ×20 (**A** and **B**).

Ym1 mRNA expression was increased only in male *βENaC* MG KO mice compared with control mice. In contrast, I1α and matrix metalloproteinase 9 mRNA levels were elevated in female *βENaC* MG KO mice compared with control mice (Figure 9B).

Multiplex assays of conjunctival tissue homogenates revealed significantly increased IL-1α and KC protein levels in 5-month—old *βENaC* MG KO mice compared with control mice (Figure 9D). Female and male mice were combined for statistical analysis because of low sample numbers in each group. The remaining cytokines analyzed, including IL-1β, IL-6, IL-13, IL-17, tumor necrosis factor-α, and interferon-γ, were lower than the detection limit of the assay.

Further evidence of inflammatory cell infiltration in ocular tissues of *βENaC* MG KO mice was generated by the immunostaining for Ly-6B.2, which is a heavily glycosylated protein expressed on neutrophils, inflammatory monocytes, and some activated macrophages.[23] There was inflammatory cell infiltration in MG gland regions (Figure 10A), as well as in the conjunctival epithelium (Figure 10B) and connective tissues underneath conjunctival epithelia of *βENaC* MG KO mice.

## Conjunctival Proliferative Response to Inflammation

Ki-67 immunostaining was performed to test the hypothesis that chronic inflammation in the *βENaC* MG KO conjunctiva would be associated with epithelial proliferation and repair. An increase in Ki-67 staining was observed in the palpebral conjunctiva of *βENaC* MG KO mice compared with control mice (Figure 11).

## Changes of Cytokeratin Expression and Distribution Pattern Determined by Immunohistochemistry

Cytokeratins (CKs) are intermediate filament-forming proteins responsible for the structural integrity and function of epithelial cells. Ocular tissues exhibit a broad expression profile of cytokeratins, some of which have unique distribution patterns in cornea, conjunctiva, and MG tissue. As described above, there was a prominent epitheliopathy in conjunctival and corneal epithelial cells of *βENaC* MG KO mice. Immunohistochemistry of selected cytokeratins revealed changes of expression and localization pattern associated with disease.

CK5 was expressed widely in the corneal, conjunctival, and MG ductal epithelial cells. The expression pattern was similar in *βENaC* control and KO mice (data not shown).

CK10, a marker for keratinization, is highly expressed in the epidermis of skin tissues, including the skin of the eyelid (Figure 12A). Most CK10 expression in control mice ended at the mucocutaneous junction of the eyelid margin, with a slight distribution over the outermost superficial layer of the palpebral conjunctiva (Figure 12A). In 11-month—old *βENaC* MG KO mice, there was strong staining in several superficial layers of palpebral conjunctiva, but not in fornical and bulbar conjunctiva (Figure 12A). Positive staining for CK10 was also observed in the central corneal epithelial cells of *βENaC* MG KO mice, a finding distinctly different from control mice (Figure 12B).

CK12 is reported to be a corneal-specific cytokeratin. It was expressed exclusively by the corneal epithelial cells, but not by conjunctival or MG acinar or ductal epithelial cells, in control mice (Figure 12C). Surprisingly, in *βENaC* MG KO mice,

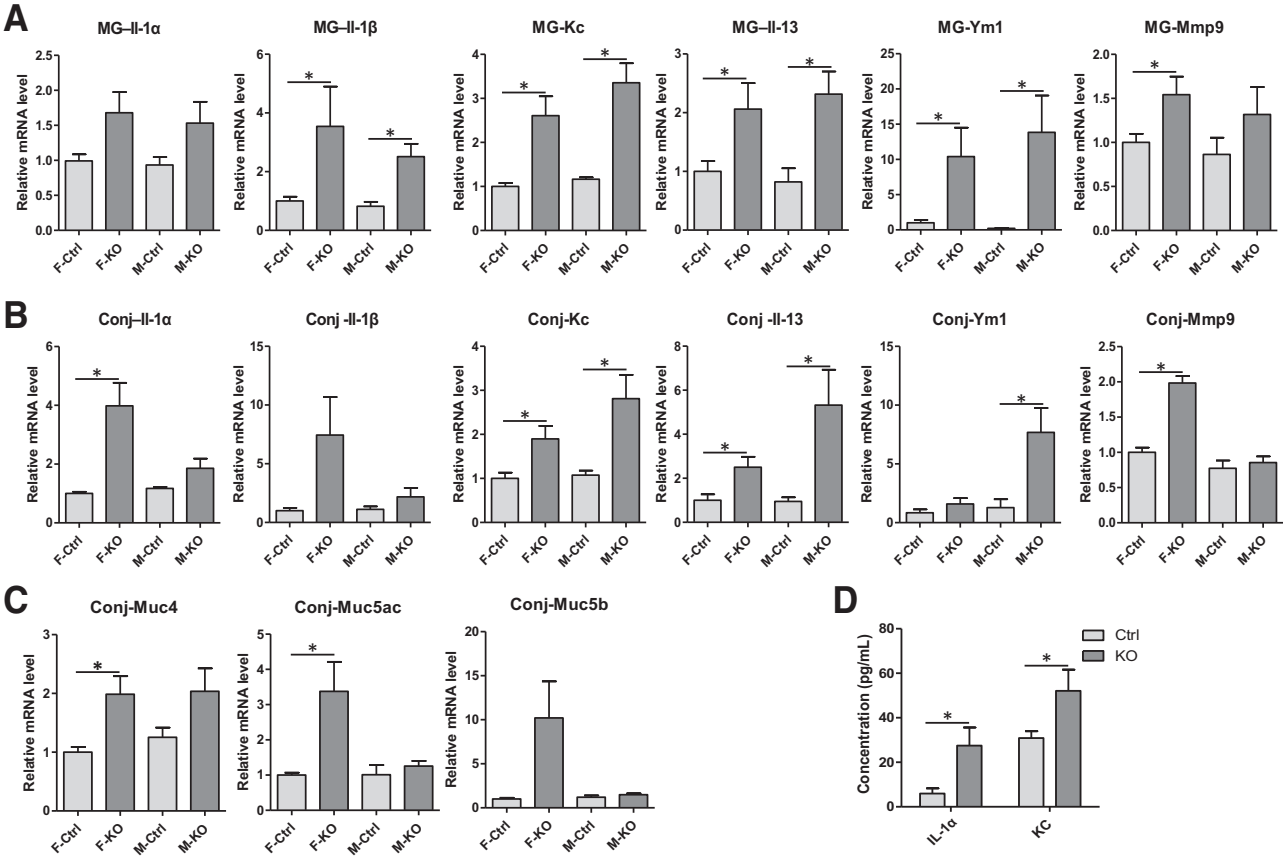


**Figure 9** Inflammation of MG and conjunctiva (Conj) induced by *βENaC* deletion in 5-month—old mice, as assessed by cytokine mRNA expression. **A:** Cytokine mRNA expression in MG. **B:** Cytokine mRNA expression in conjunctiva. **C:** Tethered (Muc4) and secretory (Muc5ac) mucin mRNA levels in female (F) and male (M) *βENaC* MG knockout (KO) mice compared with control (Ctrl) mice. **D:** Multiplex assays of conjunctival tissue homogenates for IL-1α and keratinocyte chemoattractant (KC) protein levels in *βENaC* MG KO mice compared with control mice (male and female combined). $*P < 0.05$. Mmp, matrix metalloproteinase; Ym1, Beta-N-acetylhexosaminidase Ym1.

CK12 was expressed only by the peripheral corneal epithelial cells, which were more histologically normal, but not by the central corneal epithelial cells that exhibited prominent epidermoid histological abnormalities (Figure 12C).

CK13 was highly expressed by several superficial layers of palpebral, fornical, and bulbar conjunctival epithelial cells and slightly expressed by the corneal epithelial cells in control mice (Figure 12, D and E). Intense staining was also observed in superficial layers of palpebral, fornical, and bulbar conjunctival epithelial cells of *βENaC* MG KO mice (Figure 12D). Notably, there was abnormal CK13 expression in both peripheral and central corneal epithelial cells of *βENaC* MG KO mice (Figure 12E).

CK19 appeared to be a conjunctival-specific cytokeratin. In control mice, its expression was limited to the superficial layers of conjunctival epithelial cells, with an increasing density from palpebral conjunctival to fornical to bulbar conjunctival epithelial cells (Supplemental Figure S7). No CK19 signal was observed in cornea or MG tissues in control mice. In *βENaC* MG KO mice, similar increasing staining was present ranging from eyelid wiper areas to palpebral to fornical to bulbar conjunctival epithelial cells (Supplemental Figure S7). An abnormal staining CK19 pattern, however, was observed in the cornea. CK19 was expressed by the superficial layers of both the peripheral and central corneal epithelial cells of *βENaC* MG KO, but not control, mice (Figure 12F).

Collectively, there were major changes in cytokeratin expression and localization in *βENaC* MG KO mice. The palpebral conjunctiva exhibited cutinization/keratinization, as evidenced by extension of strong expression of CK10 from the mucocutaneous junction of the eyelid margin to the palpebral conjunctiva. The central cornea was also positive for CK10. *βENaC* MG KO mouse corneal epithelial cells lost their normal expression pattern of CK12. Instead, CK13 and CK19 were expressed, suggesting conjunctival differentiation (ie, conjunctivalization) of the cornea.

## βENaC Is Involved in the Proliferation of Cultured Mouse Meibomian Gland Cells

On the basis of the localization of βENaC to the periphery of the rat MG acinus,[12] we hypothesized that ENaC was involved in MG cell proliferation processes. As noted in

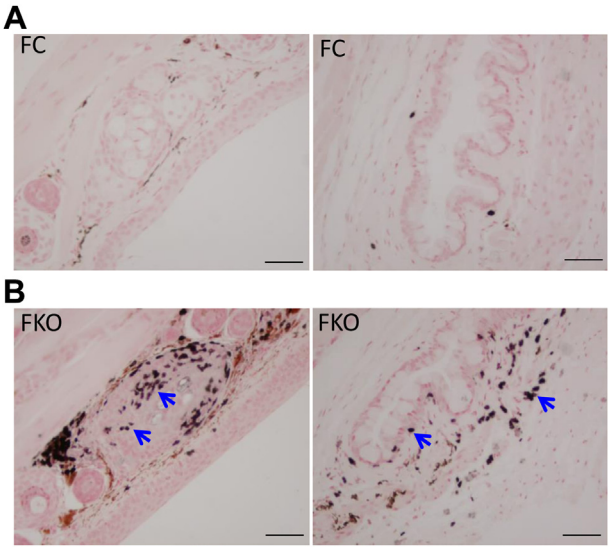


**Figure 10** Immunostaining for the inflammatory cell marker Ly-6B.2. **A:** Three-month–old female control (FC) mice. **B:** Three-month–old female *βENaC* MG KO (FKO) mouse. Inflammatory cells were observed infiltrating the MG ductal epithelial cells (**left panel**) and the conjunctival epithelia and connective tissues underneath conjunctival epithelia (**right panel**) of *βENaC* MG KO, but not control, mice. **Arrows** indicate positive staining. Scale bars = 50 μm (**A** and **B**). Original magnification, ×20 (**A** and **B**).

*Materials and Methods*, a mouse cell culture was developed for MG cells. In this system, MG cells were co-cultured with mitomycin C–treated 3T3 SA feeder cells in combination with a ρ kinase inhibitor.[24] Real-time RT-PCR assay of MG cells confirmed the absence of βENaC mRNA in cell cultures derived from *βENaC* MG KO mice (Figure 13A).

WST-1 cell proliferation assays revealed lower proliferative rates in the MG cells derived from male *βENaC* MG KO than control mice and a similar trend for female mice (Figure 13B). Furthermore, 10 μmol/L benzamil reduced proliferation rates significantly in both female and male control MG cells after 2-hour exposure (Figure 12B). In contrast, no response was observed in the addition of benzamil in the MG cells derived from female and male *βENaC* MG KO mice at this time point.

## Discussion

To study the role of βENaC in MG physiology and PHA 1–associated dysfunction *in vivo*, a conditional *βENaC* MG KO mouse model was generated. βENaC expression was selectively deleted in the murine MG, preserving βENaC expression in the conjunctiva and cornea. Strikingly, the *βENaC* MG KO mice exhibited both atrophy of MG and a phenotype of MG orifice obstruction with white toothpaste–like secretions that appeared as early as 7 weeks of life. In older mice, in addition to the prominent MG obstructive phenotype and swollen eyelid margins, there were striking corneal pathologies, including corneal opacification, ulceration, perforation, neovascularization, and ectasia.

The holocrine secretion mode of MG and the localization of βENaC to the peripheral area of MG acinar cells suggested that the MG atrophy associated with *βENaC* deletion was linked to abnormal proliferation and regeneration of MG acinar cells independent of transepithelial ion transport.[12] Indeed, studies of cultured mouse MG cells revealed lower proliferative capacities of MG cells derived from *βENaC* MG KO than control mice. In addition, inhibition of ENaC by benzamil suppressed proliferation of MG cells cultured from control mice but not cells from *βENaC* MG KO mice. These studies lend support to the hypothesis that βENaC plays a role in normal MG function through its action in proliferation and regeneration of MG acinar cells, processes absolutely required for the holocrine secretion process.

The data from our mouse studies phenocopied the observed ocular phenotype of human PHA 1 subjects. The early life development of whitish, thick meibum obstruction of MG ducts in mice rather precisely mimicked observations in human PHA 1 subjects. The classic human PHA 1 phenotype, including high sweat sodium chloride values and renal salt wasting, reflects ENaC dysfunction in relation to ductal transepithelial ion transport. In contrast, our data suggest that the βENaC dysfunction in the eyelid reflects MG acinar atrophy rather than an MG ductal ion transport dysfunction. Future studies of MG morphology and proliferative capacity in human PHA 1 subjects may be informative.

Our findings have relevance to a persistent controversy surrounding the pathogenesis of DED. Namely, it is difficult to discern whether dryness, usually defined as tear film

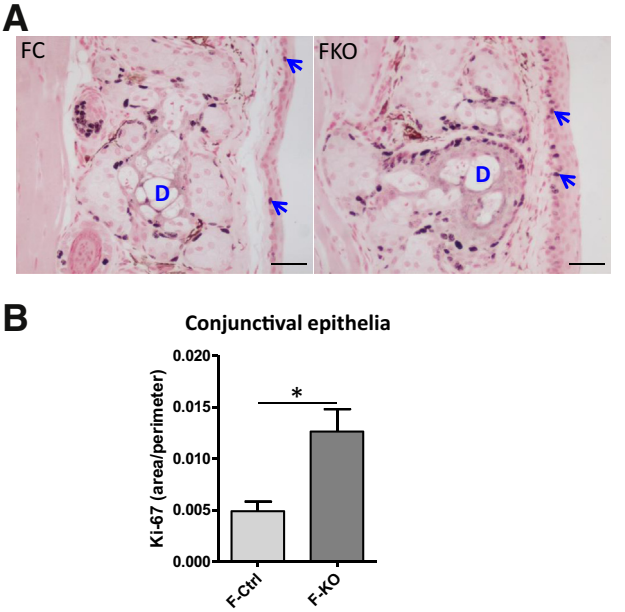


**Figure 11** Immunostaining of Ki-67 in 3-month–old female mouse conjunctival epithelia. **A:** Ki-67 localization to the basal layer of conjunctival epithelia of both female control (FC) and *βENaC* MG KO (FKO) mice, as indicated by **arrows**. **B:** Ki-67 immunostaining intensity measurements with ImageJ reveal an increased level of Ki-67 in the conjunctival epithelia of *βENaC* MG KO compared with control mice. *$P < 0.05$. Scale bars = 50 μm (**A**). Original magnification, ×20 (**A**). D, duct.

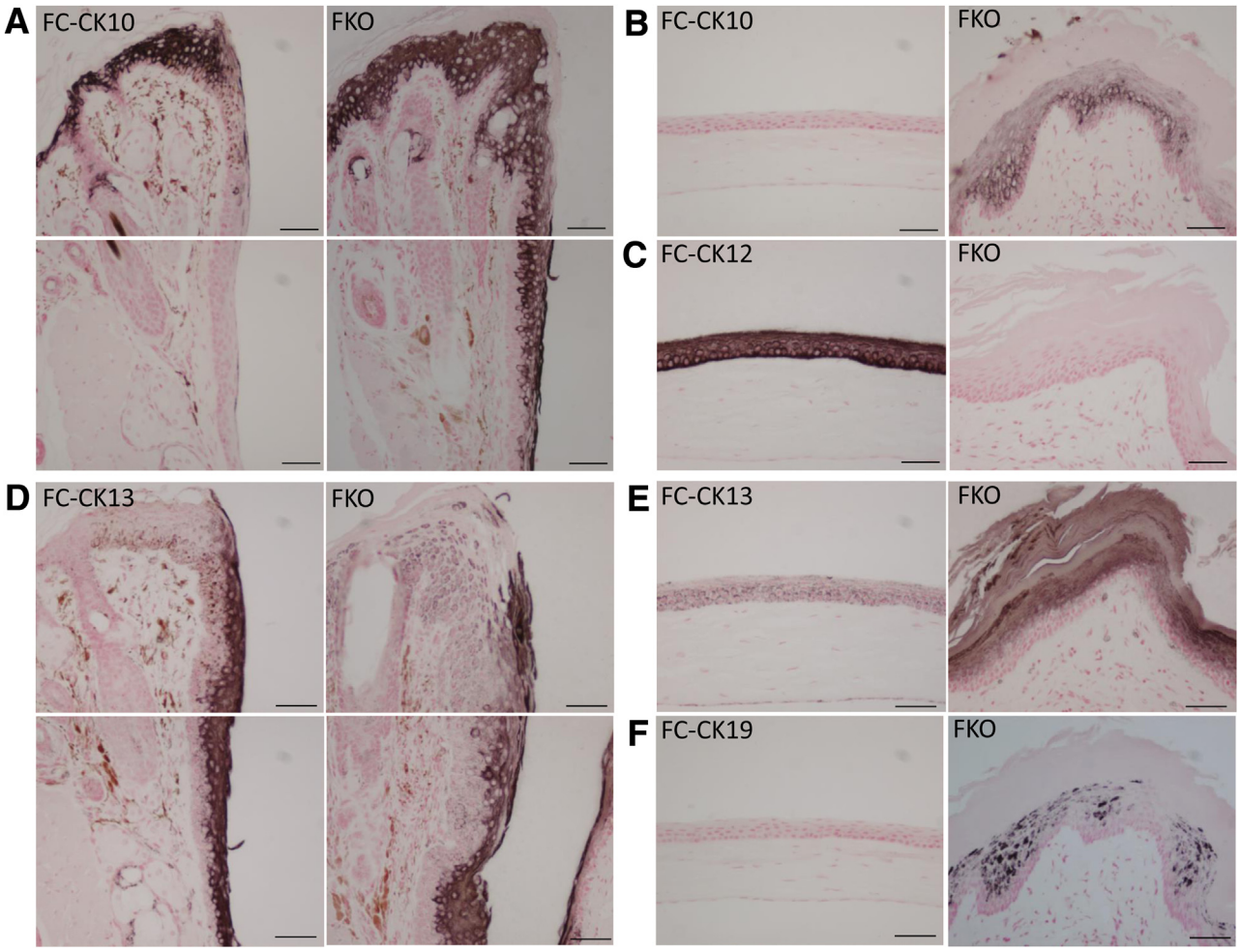


**Figure 12** Immunostaining of cytokeratins (CKs) in ocular tissues of 11-month—old female control (FC) and *βENaC* MG KO (FKO) mice. **A:** CK10 staining is observed in the eyelid skin region in control mice. There is strong aberrant CK10 immunostaining in the epithelial cells surrounding the MG orifice, eyelid wiper region, and superficial layers of palpebral conjunctiva, but not fornical and bulbar conjunctiva, in *βENaC* MG KO mice. **B:** Positive staining for CK10 is also observed in the central corneal epithelial cells of *βENaC* MG KO, but not control, mice. **C:** The cornea-specific cytokeratin, CK12, is expressed uniformly in control mice but is not expressed in the central cornea of *βENaC* MG KO mice. **D:** CK13 is highly expressed in the superficial layers of palpebral, fornical, and bulbar conjunctival epithelial cells in control, but not *βENaC* MG KO, mice. **E:** Increased CK13 expression is observed in both peripheral and central corneal epithelial cells of *βENaC* MG KO compared with control mice. **F:** CK19 is not expressed in control corneas but is aberrantly expressed by the superficial layers of both the peripheral and central corneal epithelial cells of *βENaC* MG KO mice. Scale bars = 50 μm (**A**—**F**). Original magnification, ×20 (**A**—**F**).

hyperosmolarity, precedes and causes an ocular surface inflammatory syndrome or whether dryness is a consequence of a disease initiated by an inflammatory stimulus.[25—27] This controversy reflects the fact that once the homeostasis of ocular surface health is disturbed and the vicious cycle of dryness, inflammation, and epithelial remodeling has been initiated, it is difficult to identify the entry point for this cycle. The challenge of identifying cause is magnified when environmental challenges are superimposed on a compromised ocular surface, which promotes persistence and/or acceleration of this cycle. Increased osmolality and inflammatory cytokine expression in the tears, increased cytokine expression in ocular tissues, and epithelial remodeling have all been reported to closely track the progression of MGD-induced DED.[28—30]

The design of our model may provide insight into the sequence of tear film hyperosmolarity (dryness) versus inflammation in producing DED. The initiating lesion was deletion of expression of an ion channel in the MG acinus. The effect of βENaC deletion was to produce progressive acinar atrophy with modest inflammation, ductal enlargement, and epithelial cell stratification. More important, the genetic deletion of *βENaC* was restricted to the MG gland and did not involve the ocular surface.

We speculated that the loss of MG acinar function, by reducing/deleting the lipid barrier at the tear film surface to evaporation, would produce a hyperosmolal tear film. Evidence for evaporative water loss from tears of *βENaC* KO mice was evident from increased tear fluid sodium concentrations. This finding, plus the increase in sialic acid/urea ratio (a marker of mucin concentration),[18] linked abnormal MG function to an abnormality of tear fluid concentration/osmolality. Interestingly, tear production in female βENaC KO mice was greater than in control mice.

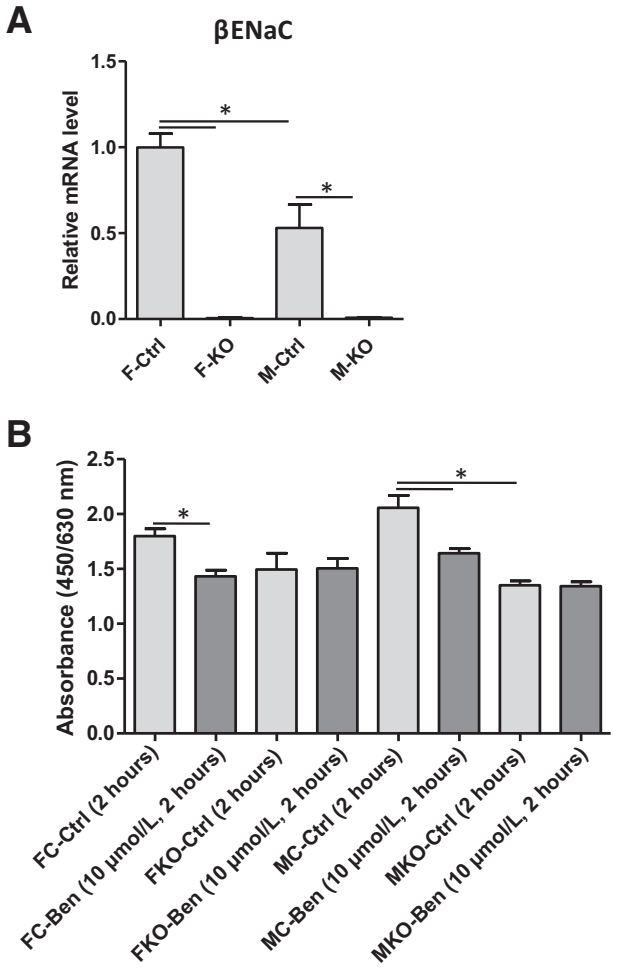


**Figure 13** Primary mouse MG cell culture. **A:** Real-time RT-PCR assay confirms the deletion of βENaC mRNA in MG cells derived from both female (F-KO) and male (M-KO) *βENaC* MG KO mice. The level of βENaC mRNA is significantly higher in MG cells derived from female control (F-Ctrl) than male control (M-Ctrl) mice. **B:** WST-1 cell proliferation assays reveal lower proliferative rates in the MG cells derived from male *βENaC* MG KO than control mice (MC-Ctrl versus MKO-Ctrl). Furthermore, 10 μmol/L benzamil (Ben; an ENaC inhibitor) reduces proliferation rates significantly in both female and male control MG cells after 2-hour exposure (FC-Ctrl versus FC-Ben, and MC-Ctrl versus MC-Ben), but not in the βENaC MG KO cells. $*P < 0.05$.

It is possible that enhanced aqueous tear production in βENaC KO mice reflected a compensatory response to the loss of the lipid layer, triggered by hyperosmolality as a constant stimulus to tear secretion. A similar phenomenon has been reported in MGD patients, who exhibit increased tear production compared with non−Sjögren syndrome aqueous-deficient dry eye patients.[31]

The MG abnormality and dysfunction caused by *βENaC* deletion resulted in disruption of the ocular surface homeostasis and development of corneal and conjunctival inflammation in the presence of normal conjunctival/corneal βENaC expression. Longitudinal studies revealed histological findings in the conjunctival tissues of inflammatory cell infiltration, positive immunostaining for the inflammatory cell marker Ly-6B.2, and increased cytokine/chemokine gene and protein expression. These findings were associated with progressive ocular surface disease, including proliferation, hyperstratification, and hyperkeratinization of conjunctival and corneal epithelia, goblet cell hyperplasia, and neovascularization. These histological changes were accompanied by changes in epithelial cytokeratin immunostaining typical of human DED. The palpebral conjunctiva exhibited cutinization/keratinization, as evidenced by strong expression of CK10 extending from the mucocutaneous junction of the eyelid margin to the palpebral conjunctiva. The corneal epithelial cells lost their normal expression pattern of CK12. In the place of CK12, corneal epithelial cells expressed CK10, CK13, and CK19, suggesting conjunctivalization and epidermalization of cornea.[32] Although it has been well documented that normal MG function is fundamental in maintaining the ocular surface health, the *βENaC* MG KO mouse model provided evidence for a progression from a selective loss of normal MG function to severe ocular surface damage mediated, at least in part, by ocular surface desiccation (dryness) rather than primary ocular surface inflammation.

Both evaporative and aqueous volume depletion DED are more prevalent in female than male human subjects.[33] The phenotype of MGD and severe ocular surface damage was also more penetrant in female than male *βENaC* MG KO mice. Sex steroid hormone receptors are widely distributed in ocular tissues, including conjunctiva, cornea, MG, lacrimal gland, lens, retina, and ciliary body.[34−37] It has been suggested that the ocular tissues are susceptible to hormonal actions because of local synthesis of sex hormones. In MG, androgens have been proved to exert a beneficial influence on the differentiation, lipid production, and secretion from meibocytes of MG, whereas estrogens produce inhibitory effects on MG function.[38] It is not clear how loss of βENaC function interacts with sex hormones to produce MGD. There were higher levels of α, β, and γ ENaC mRNA expression in 5-month−old female than male control mice. In addition, decreased levels of α and γ ENaC mRNA expression were evident in 5-month−old female, but not male, *βENaC* MG KO mice compared with control mice. It is likely that female MG mice may need a higher level of ENaC function than males to generate the levels of MG proliferation required for normal meibum production.

There has been increased research, clinical interest, and recognition of MGD. The development of MGD mouse models provides a tool for studying the pathophysiology of the disease. Animal models that exhibit abnormal MGs have been reported previously, which include cauterization of the MG orifices,[39] topical application of epinephrine,[40] hairless mice fed with a lipid-limited diet,[41] deletion of fatty acid transport protein 4,[42] and mutations of the ectodermal dysplasia gene.[43,44] The *βENaC* MG KO mouse model resembles human PHA 1 subjects with ocular pathologies and a pathognomonic MG phenotype (ie, obstruction at the gland orifice, ductal enlargement, inflammation, atrophy of acini, and a swollen eyelid margin).[8−10,45−47] These features of the *βENaC* MG KO mouse make it an attractive model to investigate the effect of novel

therapies to slow the progression of MG and ocular surface disease in subjects with PHA 1.

In conclusion, this study has provided evidence that βENaC is critical in normal mouse MG acinar function. Loss of βENaC function in mice produced MG acinar atrophy, ductal obstruction, and eventually severe ocular surface disease. These studies may contribute to an understanding of the pathogenesis and as a model for therapy of PHA 1 disease.

## Acknowledgments

We thank Elke Kretschmer for processing tissues for electron microscopy, Jörg Pekarsky for editing the scanning electron microscopy and transmission electron microscopy figures, Dr. Brian C. Gilger for critically reviewing and commenting on the manuscript, Eric C. Roe for editing the manuscript, University of North Carolina Cystic Fibrosis Research Center/Marsico Lung Institute Molecular Core and Michael Hooker Microscopy Core for facility access, Carlton W. Anderson for performing multiplex assays, and Tara N. Guhr Lee for assisting in tear analysis.

## Supplemental Data

Supplemental material for this article can be found at *https://doi.org/10.1016/j.ajpath.2017.09.016*.

## References

1. Green-Church KB, Butovich I, Willcox M, Borchman D, Paulsen F, Barabino S, Glasgow BJ: The international workshop on meibomian gland dysfunction: report of the subcommittee on tear film lipids and lipid-protein interactions in health and disease. Invest Ophthalmol Vis Sci 2011, 52:1979−1993
2. Schaumberg DA, Nichols JJ, Papas EB, Tong L, Uchino M, Nichols KK: The international workshop on meibomian gland dysfunction: report of the subcommittee on the epidemiology of, and associated risk factors for, MGD. Invest Ophthalmol Vis Sci 2011, 52:1994−2005
3. Knop E, Knop N, Millar T, Obata H, Sullivan DA: The international workshop on meibomian gland dysfunction: report of the subcommittee on anatomy, physiology, and pathophysiology of the meibomian gland. Invest Ophthalmol Vis Sci 2011, 52:1938−1978
4. Schaumberg DA, Sullivan DA, Buring JE, Dana MR: Prevalence of dry eye syndrome among US women. Am J Ophthalmol 2003, 136:318−326
5. Schaumberg DA, Dana R, Buring JE, Sullivan DA: Prevalence of dry eye disease among US men: estimates from the Physicians' Health Studies. Arch Ophthalmol 2009, 127:763−768
6. Krenzer KL, Dana MR, Ullman MD, Cermak JM, Tolls DB, Evans JE, Sullivan DA: Effect of androgen deficiency on the human meibomian gland and ocular surface. J Clin Endocrinol Metab 2000, 85: 4874−4882
7. Den S, Shimizu K, Ikeda T, Tsubota K, Shimmura S, Shimazaki J: Association between meibomian gland changes and aging, sex, or tear function. Cornea 2006, 25:651−655
8. Ainsworth JR, Ramsay AS, Galea P, Diaper C: Disordered meibomian gland function in pseudohypoaldosteronism. Arch Ophthalmol 1996, 114:1018−1019
9. Eliwa MS, El-Emmawie AH, Saeed MA: Ocular and skin manifestations in systemic pseudohypoaldosteronism. BMJ Case Rep 2014, 2014. bcr2014203741
10. Nasir A, Najab IA: Unique eyelid manifestations in type 1 pseudohypoaldosteronism. Arch Dis Child Fetal Neonatal Ed 2012, 97:F462
11. Garty H, Palmer LG: Epithelial sodium channels: function, structure, and regulation. Physiol Rev 1997, 77:359−396
12. Yu D, Davis RM, Aita M, Burns KA, Clapp PW, Gilmore RC, Chua M, O'Neal WK, Schlegel R, Randell SH, Boucher RC: Characterization of rat meibomian gland ion and fluid transport. Invest Ophthalmol Vis Sci 2016, 57:2328−2343
13. Xu W, Hong SJ, Zeitchek M, Cooper G, Jia S, Xie P, Qureshi HA, Zhong A, Porterfield MD, Galiano RD, Surmeier DJ, Mustoe TA: Hydration status regulates sodium flux and inflammatory pathways through epithelial sodium channel (ENaC) in the skin. J Invest Dermatol 2015, 135:796−806
14. Justet C, Evans F, Vasilskis E, Hernandez JA, Chifflet S: ENaC contribution to epithelial wound healing is independent of the healing mode and of any increased expression in the channel. Cell Tissue Res 2013, 353:53−64
15. Han SB, Hyon JY, Woo SJ, Lee JJ, Kim TH, Kim KW: Prevalence of dry eye disease in an elderly Korean population. Arch Ophthalmol 2011, 129:633−638
16. Merillat AM, Charles RP, Porret A, Maillard M, Rossier B, Beermann F, Hummler E: Conditional gene targeting of the ENaC subunit genes Scnn1b and Scnn1g. Am J Physiol Renal Physiol 2009, 296:F249−F256
17. Dursun D, Wang M, Monroy D, Li DQ, Lokeshwar BL, Stern ME, Pflugfelder SC: A mouse model of keratoconjunctivitis sicca. Invest Ophthalmol Vis Sci 2002, 43:632−638
18. Esther CR Jr, Hill DB, Button B, Shi S, Jania C, Duncan EA, Doerschuk CM, Chen G, Ranganathan S, Stick SM, Boucher RC: Sialic acid-to-urea ratio as a measure of airway surface hydration. Am J Physiol Lung Cell Mol Physiol 2017, 312:L398−L404
19. Esther CR Jr, Boysen G, Olsen BM, Collins LB, Ghio AJ, Swenberg JW, Boucher RC: Mass spectrometric analysis of biomarkers and dilution markers in exhaled breath condensate reveals elevated purines in asthma and cystic fibrosis. Am J Physiol Lung Cell Mol Physiol 2009, 296:L987−L993
20. Priebe M, Muller-Hulsbeck S, Jahnke T, Charalambous N, Hedderich J, Heller M, Paulsen FP: Influence of various cell-detachment solutions on endothelial cells after catheter abrasion for prosthesis colonization prior to implantation. J Biomed Mater Res A 2006, 78:399−406
21. Hampel U, Schroder A, Mitchell T, Brown S, Snikeris P, Garreis F, Kunnen C, Willcox M, Paulsen F: Serum-induced keratinization processes in an immortalized human meibomian gland epithelial cell line. PLoS One 2015, 10:e0128096
22. Jensen EC: Quantitative analysis of histological staining and fluorescence using ImageJ. Anat Rec (Hoboken) 2013, 296:378−381
23. Rosas M, Thomas B, Stacey M, Gordon S, Taylor PR: The myeloid 7/4-antigen defines recently generated inflammatory macrophages and is synonymous with Ly-6B. J Leukoc Biol 2010, 88: 169−180
24. Suprynowicz FA, Upadhyay G, Krawczyk E, Kramer SC, Hebert JD, Liu X, Yuan H, Cheluvaraju C, Clapp PW, Boucher RC Jr, Kamonjoh CM, Randell SH, Schlegel R: Conditionally reprogrammed cells represent a stem-like state of adult epithelial cells. Proc Natl Acad Sci U S A 2012, 109:20035−20040
25. Stevenson W, Chauhan SK, Dana R: Dry eye disease: an immune-mediated ocular surface disorder. Arch Ophthalmol 2012, 130:90−100
26. Luo L, Li DQ, Corrales RM, Pflugfelder SC: Hyperosmolar saline is a proinflammatory stress on the mouse ocular surface. Eye Contact Lens 2005, 31:186−193
27. Yagci A, Gurdal C: The role and treatment of inflammation in dry eye disease. Int Ophthalmol 2014, 34:1291−1301
28. Baudouin C, Messmer EM, Aragona P, Geerling G, Akova YA, Benitez-del-Castillo J, Boboridis KG, Merayo-Lloves J, Rolando M, Labetoulle M: Revisiting the vicious circle of dry eye disease: a focus on the pathophysiology of meibomian gland dysfunction. Br J Ophthalmol 2016, 100:300−306

29. Enriquez-de-Salamanca A, Castellanos E, Stern ME, Fernandez I, Carreno E, Garcia-Vazquez C, Herreras JM, Calonge M: Tear cytokine and chemokine analysis and clinical correlations in evaporative-type dry eye disease. Mol Vis 2010, 16:862−873
30. Jackson DC, Zeng W, Wong CY, Mifsud EJ, Williamson NA, Ang CS, Vingrys AJ, Downie LE: Tear interferon-gamma as a biomarker for evaporative dry eye disease. Invest Ophthalmol Vis Sci 2016, 57:4824−4830
31. Arita R, Morishige N, Koh S, Shirakawa R, Kawashima M, Sakimoto T, Suzuki T, Tsubota K: Increased tear fluid production as a compensatory response to meibomian gland loss: a multicenter cross-sectional study. Ophthalmology 2015, 122:925−933
32. Tektas OY, Yadav A, Garreis F, Schlotzer-Schrehardt U, Schicht M, Hampel U, Brauer L, Paulsen F: Characterization of the mucocutaneous junction of the human eyelid margin and meibomian glands with different biomarkers. Ann Anat 2012, 194:436−445
33. The epidemiology of dry eye disease: report of the Epidemiology Subcommittee of the International Dry Eye WorkShop (2007). Ocul Surf 2007, 5:93−107
34. Sullivan DA, Jensen RV, Suzuki T, Richards SM: Do sex steroids exert sex-specific and/or opposite effects on gene expression in lacrimal and meibomian glands? Mol Vis 2009, 15:1553−1572
35. Spelsberg H, Klueppel M, Reinhard T, Glaeser M, Niederacher D, Beckmann MW, Sundmacher R: Detection of oestrogen receptors (ER) alpha and beta in conjunctiva, lacrimal gland, and tarsal plates. Eye (Lond) 2004, 18:729−733
36. Schirra F, Suzuki T, Dickinson DP, Townsend DJ, Gipson IK, Sullivan DA: Identification of steroidogenic enzyme mRNAs in the human lacrimal gland, meibomian gland, cornea, and conjunctiva. Cornea 2006, 25:438−442
37. Rocha EM, Wickham LA, da Silveira LA, Krenzer KL, Yu FS, Toda I, Sullivan BD, Sullivan DA: Identification of androgen receptor protein and 5alpha-reductase mRNA in human ocular tissues. Br J Ophthalmol 2000, 84:76−84
38. Schirra F, Richards SM, Liu M, Suzuki T, Yamagami H, Sullivan DA: Androgen regulation of lipogenic pathways in the mouse meibomian gland. Exp Eye Res 2006, 83:291−296
39. Gilbard JP, Rossi SR, Heyda KG: Tear film and ocular surface changes after closure of the meibomian gland orifices in the rabbit. Ophthalmology 1989, 96:1180−1186
40. Jester JV, Rife L, Nii D, Luttrull JK, Wilson L, Smith RE: In vivo biomicroscopy and photography of meibomian glands in a rabbit model of meibomian gland dysfunction. Invest Ophthalmol Vis Sci 1982, 22:660−667
41. Miyake H, Oda T, Katsuta O, Seno M, Nakamura M: Meibomian gland dysfunction model in hairless mice fed a special diet with limited lipid content. Invest Ophthalmol Vis Sci 2016, 57:3268−3275
42. Lin MH, Hsu FF, Miner JH: Requirement of fatty acid transport protein 4 for development, maturation, and function of sebaceous glands in a mouse model of ichthyosis prematurity syndrome. J Biol Chem 2013, 288:3964−3976
43. Wang YC, Li S, Chen X, Ma B, He H, Liu T, Yu J, Zhang L, Chen Y, Liu Z, Li W: Meibomian gland absence related dry eye in ectodysplasin A mutant mice. Am J Pathol 2016, 186:32−42
44. Cui CY, Smith JA, Schlessinger D, Chan CC: X-linked anhidrotic ectodermal dysplasia disruption yields a mouse model for ocular surface disease and resultant blindness. Am J Pathol 2005, 167:89−95
45. Nien CJ, Massei S, Lin G, Nabavi C, Tao J, Brown DJ, Paugh JR, Jester JV: Effects of age and dysfunction on human meibomian glands. Arch Ophthalmol 2011, 129:462−469
46. Foulks GN, Bron AJ: Meibomian gland dysfunction: a clinical scheme for description, diagnosis, classification, and grading. Ocul Surf 2003, 1:107−126
47. Obata H: Anatomy and histopathology of human meibomian gland. Cornea 2002, 21:S70−S74